Effects of neutron irradiation on magnetic first-order reversal curves in reactor pressure vessel steels

Satoru Kobayashi,[1, a)] Hiroaki Murakami,[1] Ákos Horváth,[2] László Almásy,[3] Ferenc Gillemot,[2] and Artem Feoktystov[4]

[1)] *Department of Materials Science and Engineering, Faculty of Engineering, Iwate University, Ueda 4-3-5, Morioka 020-8551, Japan*

[2)] *Centre for Energy Research, Hungarian Academy of Sciences, H-1121 Budapest, Hungary*

[3)] *Wigner Research Centre for Physics, Hungarian Academy of Sciences, H-1121 Budapest, Hungary*

[4)] *Forschungszentrum Jülich GmbH, Jülich Centre for Neutron Science (JCNS) at Heinz Maier-Leibnitz Zentrum (MLZ), 85748 Garching, Germany*

(Dated: 28 December 2019)

We report results of measurements of first-order reversal curves (FORCs) for neutron irradiated reactor pressure vessel steels to seek their possible application to a nondestructive evaluation of the irradiation hardening. We find a peak position of the FORC distribution, which is the second derivative of measured FORCs, shifts towards zero field after neutron irradiation, associated with the narrowing of the peak width. The observations indicate the progress of the magnetic softening and magnetic homogeneity under neutron irradiation. The present investigations demonstrate that FORCs can offer additional information on microstructural changes due to neutron irradiation, which can not be obtained by a conventional hysteresis method.

[a)] Electronic mail: koba@iwate-u.ac.jp

I. INTRODUCTION

Low-alloy steels subjected to irradiation by high-energy neutrons exhibit mechanical hardening, due to the formation of radiation-induced nanoscale defects such as Cu-rich precipitates, solute-vacancy clusters, dislocation loops[1]. The irradiation embrittlement for reactor pressure vessel (RPV) steels is currently evaluated as a ductile-brittle transition temperature shift obtained by a destructive Charpy impact test. However, the diminishing stock of surveillance Charpy specimens has became a crucial issue. The development of non-destructive evaluation (NDE) method is one of the solutions, because the integrity assessment of RPVs can be done semi-permanently using the same irradiated Charpy specimens.

In recent years, we have focused on magnetic hysteresis methods as one of the possible NDE methods because radiation-induced defects can act as pinning centers for domain wall movement[2]. While an increase of a major-loop coercivity, which depends on chemical compositions and neutron fluence, was observed, the coercivity was found to be strongly affected by the recovery[3]. This results in the appearance of a local maximum in the neutron fluence dependence of coercivity. Such competing microstructural change makes it difficult to precisely evaluate effects of nanoscale defects on magnetic hysteresis properties.

Among available magnetic methods, a first-order-reversal-curve (FORC) method may be useful to explore magnetic features that have complicated microstructural origin[4–6]. The FORC distribution, obtained from a mixed second derivative of reversal field and magnetic field, provides valuable information about irreversible switching process. Recent studies for permanent magnets and magnetically multi-phase materials showed that magnetic features with different microstructural origin can be evaluated separately, unlike a major hysteresis loop that reflects the average of microstructures[6].

In this study, we have performed FORC measurements for neutron-irradiated RPV model alloys to seek a possible application of FORCs to magnetic NDE.

II. EXPERIMENTAL

Three types of RPV steels listed in Table 1 were used. JRQ is the International Atomic Energy Agency (IAEA) reference material with a relatively higher Cu content for enhancing

effect of Cu-rich precipitation[7]. VVER440 and VVER1000 steels are a second and third generation Cr-Mo-V-type pressurized water reactor steel, respectively, with low Cu content[8,9]. JRQ has a bainite microstructure, whereas both VVER steels have a tempered granular bainite one. VVER1000 with higher Ni content is more sensitive to neutron irradiation than VVER440; the volume fraction of irradiation-induced nanoscale defects is higher for Ni-containing VVER1000 than for VVER440[9].

Small plate specimens with dimensions of $2 \times 12 \times 0.5$ mm^3 were neutron-irradiated at 290°C to fluences up to 4.29×10^{19} n cm^{-2} ($>$ 1MeV) in the BR2 reactor at SCK·CEN in Belgium. The irradiation condition is listed in Table 2.

TABLE I. Chemical composition of JRQ, VVER440, and VVER1000 steels (wt%)

Sample	Cu	Ni	Mn	Cr	Mo	C	Si	P	S	V	Fe
JRQ	0.14	0.84	1.40	0.12	0.50	0.18	0.25	0.019	0.004	0.003	Bal.
VVER440	0.09	0.07	0.54	2.70	0.68	0.16	0.20	0.006	0.023	0.340	Bal.
VVER1000	0.07	1.26	0.46	2.20	0.50	0.17	0.30	0.008	0.010	0.100	Bal.

Microhardness was measured with a load of 300 gf and an averaged value was obtained from approximately 16 indents for each irradiation condition. The hardness monotonically increases with neutron fluence for all the samples [Fig. 3(a)], which confirms the development of irradiation-induced nanoscale defects under the irradiation. The increase for JRQ is larger than VVER440 and VVER1000.

Magnetic measurements were carried out at room temperature using a homemade fluxmeter designed for neutron-irradiated small samples[3]. A small plate sample was attached with a U-shape Fe-Si yoke to form a closed magnetic circuit. The detail of the measurement setup

TABLE II. Neutron irradiation conditions

	Flux ($>$1 MeV) (10^{13} n cm^{-2}s^{-1})	Fluence ($>$1 MeV) (10^{19} n cm^{-2})
Irrad-1	1.57	2.97
Irrad-2	1.187	4.29

is described in Ref. 3. FORCs with different reversal fields, H_r, were measured at a field sweep rate of $dH/dt = 9$ kA/m/s; magnetic field, H, is reduced from saturation field of 23 kA/m and then increases toward 23 kA/m after H reaches H_r. This procedure was repeated with reducing H_r with a step of ~ 250 A/m. The FORCs are a function of H_r and H, and FORC distribution is defined as

$$\rho(H, H_r) = -\frac{1}{2}\frac{\partial^2 B(H, H_r)}{\partial H \partial H_r}. \quad (1)$$

FORC diagrams were plotted by using rotating axes; an interaction field axis $H_u = (H + H_r)/2$ and a switching field axis $H_c = (H - H_r)/2$. Generally, the intensity of $\rho(H_c, H_u)$ is related to irreversibility at given H_c and H_u.

Small-angle neutron scattering (SANS) measurements were performed at room temperature to investigate the evolution of irradiation-induced nanoscale defects. In order to separate magnetic and nuclear contributions, a saturation magnetic field of 2.2 T was applied along the direction perpendicular to the neutron beam. Two dimensional (2D) detector position was set at three different positions of 1.5, 8.0, and 20 m, to access q range from 0.002 to 0.3 Å^{-1}. The magnetic SANS intensities were analyzed with an analysis tool developed by Ilavsky et al.[10]

III. EXPERIMENTAL RESULTS AND DISCUSSIONS

Figure 1 shows FORC diagrams for JRQ, VVER440, and VVER1000 for the as-received (AR) and Irrad-2 conditions. In the insets FORCs for each condition are shown. Each FORC diagram has a single distribution peak on the H_c axis. In the case of JRQ, the peak position slightly shifts towards a lower H_c after neutron irradiation.

To quantitatively analyze the FORC distribution, both the switching-field distribution, $\rho(H_c)$, and the interaction-field distribution, $\rho(H_u)$, were calculated using the following equations.

$$\rho(H_c) = \int_{-\infty}^{\infty} \rho(H_c, H_u) dH_u \quad (2)$$

$$\rho(H_u) = \int_{0}^{\infty} \rho(H_c, H_u) dH_c \quad (3)$$

In Figs. 2(a) and 2(b), $\rho(H_c)$ and $\rho(H_u)$ for VVER440 are plotted, respectively, as an example. The $\rho(H_c)$ peak is asymmetric in shape and becomes narrower after neutron

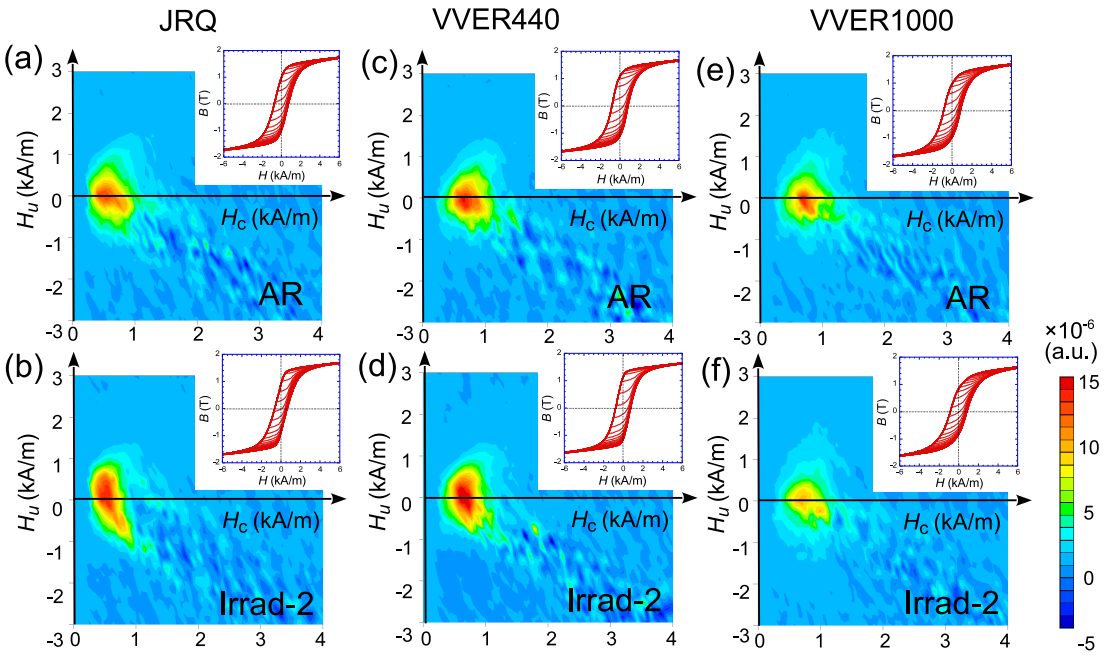

FIG. 1. FORC diagrams, taken before and after neutron irradiation (Irrad-2) for JRQ [(a), (b)], VVER440 [(c), (d)], and VVER1000 [(e), (f)]. The insets show measured FORCs, from which the FORC diagram was calculated.

irradiation, accompanying a development of the peak height. The $\rho(H_{\rm u})$ peak is located at $H_{\rm u} \sim 0$ and seems to depend on irradiation. To evaluate the position and width of the $\rho(H_{\rm c})$ and $\rho(H_{\rm u})$ peaks, $\rho(H_{\rm c})$ and $\rho(H_{\rm u})$ peaks were least-squares fitted assuming a lognormal distribution function and Lorentzian function, respectively.

It should be noted that a half-width at half-maximum (HWHM) of the $\rho(H_{\rm u})$ peak strongly depends on a contact condition for the sample surface and magnetic yoke. If the contact is poor, the resultant demagnetizing field decreases remanent flux density, leading to an increase in HWHM as shown in the inset in Fig. 2(b)[4]. Conversely, the width parameter σ of the $\rho(H_{\rm c})$ peak, which is the standard deviation of the lognormal distribution function, is weakly dependent on the contact condition. In this study, therefore, we focus only on the $\rho(H_{\rm c})$ peak.

Figures 3(b) and 3(c) summarize respectively a change of the peak position, $\Delta H_{\rm c,p}$ and that of the width parameter, $\Delta\sigma$. For both JRQ and VVER440, $\Delta H_{\rm c,p}$ and $\Delta\sigma$ decrease after neutron irradiation, whereas those for VVER1000 are almost unchanged. The decrease of the peak position for the Irrad-2 condition with respect to the AR one is $\sim$5$\pm$4 and 9$\pm$6 % for

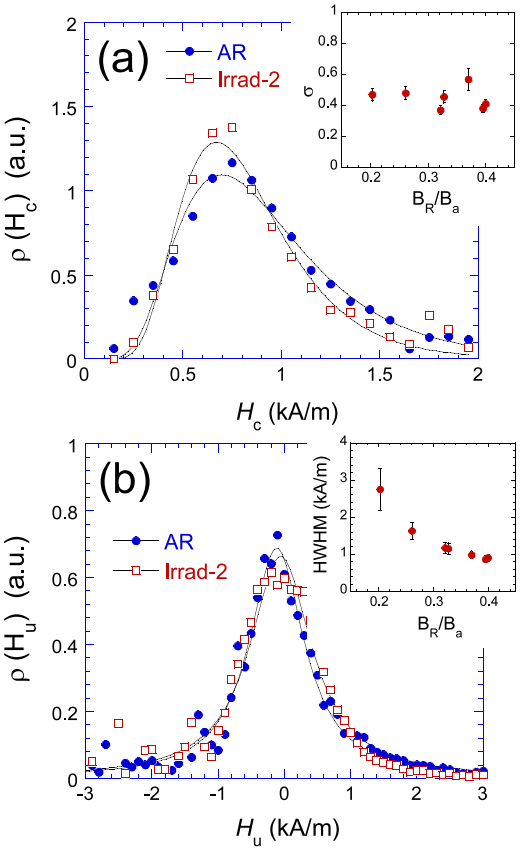

FIG. 2. FORC distribution curves along (a) $H_{\rm c}$ and (b) $H_{\rm u}$ axes, respectively, before and after neutron irradiation (Irrad-2). The data for VVER440 are shown as an example. The insets in (a) and (b) respectively show the width parameter σ and HWHM, as a function of $B_{\rm R}/B_{\rm a}$, obtained in different contact condition for the magnetic yoke and sample. Here, $B_{\rm R}$ and $B_{\rm a}$ are remanent and maximum flux densities of a major hysteresis loop, respectively.

JRQ and VVER440, respectively, and that of the width parameter for JRQ and VVER440 is $\sim$37$\pm$6 and 18$\pm$17 %, respectively. The large experimental errors are attributed to the sample dependence. The decrease of $\Delta H_{\rm c,p}$ with fluence reflects a magnetic softening by the recovery. On the other hand, a decrease of $\Delta\sigma$ suggests a narrowing distribution of reversal fields. In other words, magnetic inhomogeneity within the sample is reduced after neutron irradiation.

Figure 4 shows magnetic SANS intensities before and after neutron irradiation (Irrad-2). There was no detectable change in the magnetic SANS intensity within the measured q range after the irradiation for both VVER440 and VVER1000. Even if nanoscale defects are

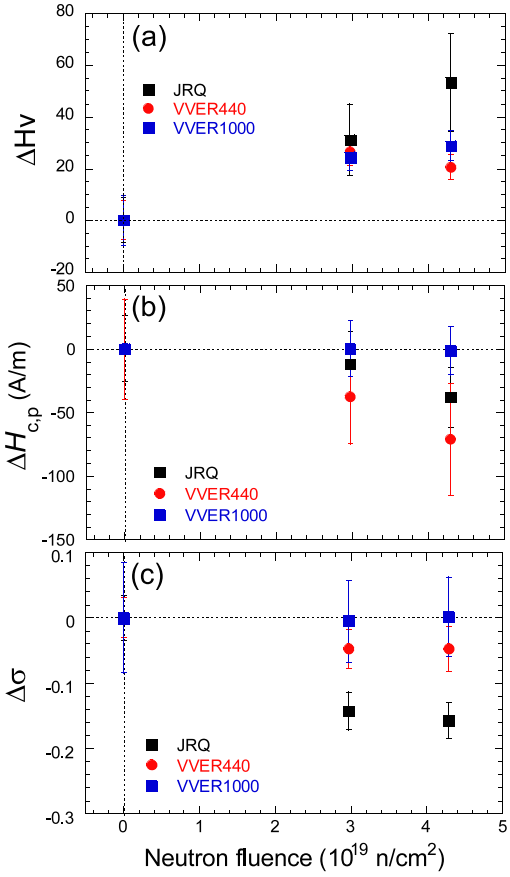

FIG. 3. Change of (a) hardness, (b) peak position and (c) width parameter of the FORC distribution peak along the H_c direction, as a function of neutron fluence.

formed, their size may be very small ($<\sim$ 1 nm) for VVER440 and VVER1000 as observed previously[8,9]. On the other hand, there is a significant increase in magnetic SANS intensity at $q = 0.1 - 0.2\text{Å}^{-1}$ for JRQ, indicating the development of nanoscale defects. Assuming a log-normal size distribution of spherical nanoscale features, the least-squares fitting to the observed SANS data yielded the size-dependent volume distribution function as shown in the inset of Fig. 4. From the figure, the volume fraction f and mean size d were obtained for JRQ; $f = 0.061$ % and 0.10 %, and $d = 2.6 \pm 0.5$ nm and 2.6 ± 0.2 nm for the Irrad-1 and Irrad-2 conditions, respectively. The values are similar to those of previous studies[12,13] and their larger values compared with those of VVER440 and VVER1000 is due to the higher Cu content for JRQ.

During neutron irradiation, various types of irradiation-induced nanoscale defects are formed. For JRQ, neutron irradiation induces the formation of Cu-rich precipitates, dis-

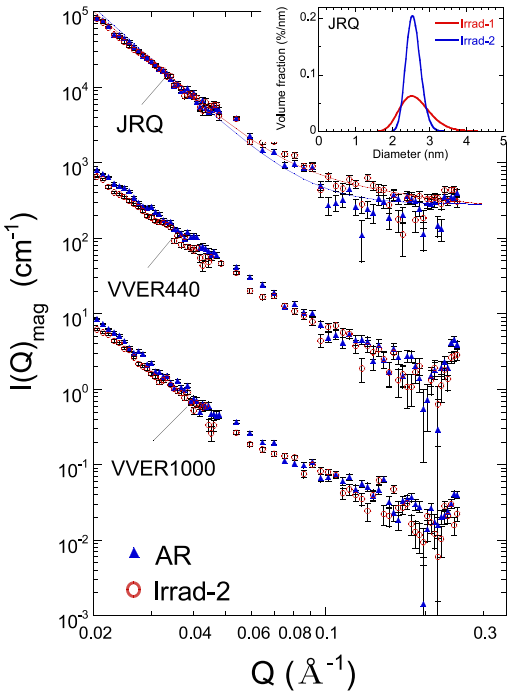

FIG. 4. Magnetic SANS intensities before and after neutron irradiation (Irrad-2). The data for JRQ and VVER440 are shifted upwards for clarity. The solid lines through the data for JRQ are least-squares fitting lines. The inset shows the volume distribution function of nanoscale features as a function of diameter after neutron irradiation for JRQ.

location loops, solute-vacancy complexes etc.[1] On the other hand, for VVER-type steels, Cu-rich precipitates, dislocation loops, and carbides are main irradiation defects, although an increasing trend of defect density with fluence is slightly different for VVER440 and VVER1000[8,9]; the density of nanoscale precipitates ($<\sim$ 2 nm) is higher for VVER1000 than for VVER440, whereas the formation of the carbides are more sensitively irradiation-induced for VVER440 as compared with VVER1000. Such materials-dependent defect density can be attributed to the composition (Table 1) and microstructure. While JRQ has a bainite microstructure, both VVER440 and VVER1000 have a tempered granular bainite one; for VVER440, a low content of proeutectoid ferrite is also included. For all the materials, Cu-rich precipitates are a primary cause of irradiation hardening in the low and medium fluence regime ($<\sim 5 \times 10^{19}$ n cm^{-2}). As described above, our SANS revealed the formation of irradiation defects for JRQ, whereas very small precipitates ($<\sim$ 1 nm) may be present for

VVER440 and VVER1000. Such nanoscale defects may contribute to the observed increase in hardness shown in Fig. 3(a).

Due to neutron irradiation, annihilation and rearrangement of pre-existing dislocations, which were produced during the manufacturing process and may distribute inhomogeneously over the sample, also occur through irradiation-induced diffusion process. This process reduces density of dislocations in the matrix[14]. Although mechanical properties such as hardness and yield stress are sensitive to nanoscale features, magnetic properties are more sensitive to internal stress due to dislocations than that of nanoscale precipitates[2,3,15]. The sensitivity of magnetic properties to dislocations originates from the fact that a Bloch wall width is a few tens nanometers ($\sim$ 40 nm for α-Fe) and is relatively wider than a size of nanoscale precipitates. This different sensitivity to microstructures results in the different fluence dependence for hardness and the FORC parameters shown in Fig. 3. The decrease in dislocation density leads to a shift of the $\rho(H_c)$ peak towards a lower H_c and a reduction of the $\rho(H_c)$ intensities at higher H_c [Fig. 2(a)]. The materials-dependent FORC properties shown in Figs. 3(b) and 3(c) might reflect a different degree of dislocation recovery. Detailed microstructural investigations for the present materials are planned to clarify the origin.

Here, it should be noted that a decrease of $\Delta\sigma$ indicates the reduced distribution of reversal fields. In other words, magnetic inhomogeneity due to dislocation is reduced after neutron irradiation. Although the formation of nanoscale defects increases microstructural inhomogeneity, the effect on magnetic properties is small due to the lesser sensitivity. Such information extracted from the width parameter can not be obtained from the conventional hysteresis measurements using a major loop.

According to previous studies for magnetic nanoparticles[4], a FORC peak along the H_u axis gives information about interparticle interactions. In the case of bulk ferromagnetic steels, information about interaction between magnetic domains and/or between magnetically soft and hard regions, may be deduced. Further FORC measurements on the present irradiated specimens for improved contact condition are planned to gain in-depth information about microstructure.

IV. SUMMARY

FORC measurements were performed for three types of RPV steels with different composition subjected to neutron irradiation. Both position and width of the FORC distribution peak changed after neutron irradiation for JRQ and VVER440, indicating the progress of magnetic softening and the magnetic homogeneity, whereas there was no significant change for VVER1000. SANS revealed the development of irradiation-induced nanoscale defects with the mean diameter of $\sim$ 2.6 nm for JRQ after neutron irradiation to the fluence of 4.29 $\times$ 10^{19} n cm^{-2}. Although microstructural changes due to the recovery and the formation of nanoscale features take place during neutron irradiation, the recovery was found to be the dominant factor affecting the FORC distribution. Nevertheless, the FORCs provide additional information on the magnetic homogeneity, which can not be obtained by conventional hysteresis measurements using a major loop.

ACKNOWLEDGEMENTS

The part of this work was performed under the Inter-University Cooperative Research Program of the International Research Center for Nuclear Materials Science, Institute for Materials Research, Tohoku University, (Proposal No. 17M0001, 18M0001). This work was supported by Grant-in-Aid for Scientific Research (B) (Grant No. 25289346) from JSPS, Japan. The part of this work was supported by JSPS and Hungarian Academy of Science under the Japan - Hungary Research Cooperative Program. The SANS data were based upon experiments performed at the KWS-1 instrument operated by JCNS at the Heinz Maier-Leibnitz Zentrum (MLZ), Garching, Germany (Proposal No. 12748). We acknowledge supports from FRM II radiation protection for SANS experiments on irradiated materials.

REFERENCES

[1]G.R. Odette, G.E. Lucas, Radiat. Eff. Def. Solids **144** (1998) 189-231.

[2]H. Kronmüler, M. Fähnle, Micromagnetism and the microstructure of ferromagnetic solids, Cambridge University press, Cambridge, 2003.

[3]S. Kobayashi, T. Yamamoto, D. Klingensmith, G.R. Odette, H. Kikuchi, and Y. Kamada, J. Nucl. Mater. **422** (2012) 158-162.

[4]C.R. Pike, A.P. Roberts, K.L. Verosub, J. Appl. Phys. **85** (1999) 6660-6667.

[5]P.-A. Chen, C.-Y. Yang, S.-J. Chang, M.-H. Lee, N.-K. Tang, S.-C. Yen, Y.-C. Tseng, J. Mag. Mag. Mater. **370** (2014) 45-53.

[6]B.C. Dodrill, J. Lindemuth, C. Radu, H. Reichard, MRS Bulletin **40** (2015) 903-904.

[7]International Atomic Energy Agency, IAEA-TECDOC-1230, Vienna (2001).

[8]E.A. Kuleshova, B.A. Gurovich, Ya.I. Shtrombakh, D.Yu. Erak, O.V. Lavrenchuk, J. Nucl. Mater. **300** (2002) 127-140.

[9]J. Bohmert, H.-W. Viehrig, A. Ulbricht, J. Nucl. Mater. **297** (2001) 251-261.

[10]J. Ilavsky, P.R. Jemian, J. Appl. Cryst. **42** (2009) 347-353.

[11]S. Kobayashi, F. Gillemot, A. Horvath, M. Horvath, L. Almasy, Q. Tian, A. Feoktystov, AIP Adv. **7** (2017) 056002.

[12]A. Ulbricht and J. Bohmert, Physica B **350** (2004) e483-e486.

[13]K. Fukuya, K. Ohno, H. Nakata, S. Dumbill, J.M. Hyde, J. Nucl. Mater. **312** (2003) 163-173.

[14]T. Páv, J. Kočík, E. Keilová, ASTM STP **1170** (1993) 300-308.

[15]S. Kobayashi, R. Kawagoe, H. Murakami, K. Ohishi, Y. Kawamura, J. Suzuki, Philos. Mag. Lett. **99** (2019) 217-225.